

Effect of Microstructure and Horizontal Inhomogeneity of Broken Cirrus Clouds on Mean Solar Radiative Fluxes in the Visible Wavelength Region: Results of Numerical Simulation

T. B. Zhuravleva^{a, *} and I. M. Nasrtdinov^{a, **}

^a V.E. Zuev Institute of Atmospheric Optics, Siberian Branch, Russian Academy of Sciences, Tomsk, 634055 Russia

*e-mail: ztb@iao.ru

**e-mail: wizard@iao.ru

Received July 14, 2021; revised July 14, 2021; accepted August 10, 2021

Abstract—We present the results from statistical simulation of the albedo and diffuse transmission of the atmosphere in the visible wavelength region in the presence of overcast and broken cirrus clouds. The main numerical experiments were performed using the third version of the model proposed by B.A. Baum, P. Yang, A.J. Heymsfield et al. (a mixture of particles of different shapes and sizes with a very rough surface). To estimate the effects of the random cloud geometry on the solar radiative transfer in the atmosphere, we used the method of closed equations, proposed by G.A. Titov, and developed within the model based on the Poisson point fluxes on straight lines. Analysis of how the microstructure of cirrus clouds influences the ensemble-averaged albedo and diffuse transmission at moderate cloud fractions showed that the average value of the uncertainty due to the lack of information on the particle shape and size is within $\sim \pm 2\%$. This value is comparable to the effect of the random geometry in optically thin clouds; while in optically dense clouds the range of errors, caused by the neglect of the horizontal inhomogeneity, increases and is $\sim \pm 5\%$ in albedo calculations, with underestimation of diffuse transmission by $\sim 10\text{--}20\%$.

Keywords: cirrus cloud models, Monte Carlo method, effects of cloud random geometry, Poisson model, solar radiative fluxes in the visible wavelength region

DOI: 10.1134/S1024856021060294

INTRODUCTION

Despite the fact that cirrus clouds are recognized to appreciably affect the Earth's climate system by regulating the radiative energy balance of the atmosphere [1, 2], our fundamental understanding of their microphysical, optical, and radiative properties is still quite limited. The discrepancies between simulations within climate models and observations (see, e.g., [3]) are not only due to problems in reproducing such cloud characteristics as the frequency of occurrence, seasonal variations, position of cloud layer in the atmosphere, etc., but also to insufficiently realistic assumptions on the microphysical characteristics of cirrus clouds, as well as to radiation codes used in operational algorithms of retrieving cloud parameters and in climate models.

Operational algorithms for retrieving cloud characteristics from remote sensing data (and, in particular, optical thickness and particle size) assume that each pixel is horizontally homogeneous, and the radiation interaction between neighboring pixels is absent. The effect the neglect of the real inhomogeneous cloud structure has on retrievals was studied in several works. Most of them addressed optically dense liquid water

clouds [4–9]; however, analysis shows that the horizontal inhomogeneity of the cloud field can also show up in retrievals in the presence of optically thin ice clouds [10–12].

Because cirrus clouds may be a cause for sign reversal of the cloud radiative forcing [13], intense research has been conducted in the two recent decades to estimate how the shape and sizes of ice particles influence the formation of broadband fluxes of solar radiation. Some of these works in this research direction have been performed using the horizontally homogeneous (1D) model of the atmosphere [14, 15]. However, experimental data accumulated to date show that this research can account for the effect of such a factor as the inhomogeneous structure of (3D) clouds using cloud realizations, either constructed on the basis of radar, lidar, and radiometric measurements [16–18], or constructed within new stochastic models of cirrus clouds [19, 20]. In particular, Buschmann et al. showed [16] that, in inhomogeneous cirrus clouds with cloud optical thickness (COT) less than five and the relative value of COT variations of less than 0.2, the relative error in the calculations of broadband radiative fluxes, caused by the use of a 1D model, does not

exceed $\pm 10\%$. Results of Carlin et al. [17] suggest that the deviation of the flux of upward solar radiation at the top of the atmosphere (TOA), caused by the stochastic cloud structure, reaches 15 W/m^2 . Estimates, obtained using generator of cloud scenes of cumulus, stratocumulus, and cirrus clouds 3DCLOUD [20], showed that the brightness temperature at the TOA in the calculations with 1D and 3D models, can differ by 15 K [21]; while in the visible wavelength region, the difference in cloud reflectance is determined by the spatial resolution of the model and, depending on the COT and observation/illumination conditions, can reach tens of percent [11].

In the publications mentioned above, the effect of the inhomogeneous cloud structure was studied using cloud realizations where the horizontal inhomogeneity of the field is caused by fluctuations in optical characteristics and concerns mainly the broadband radiative fluxes. The purpose of this work is to compare the effects of two different factors, i.e., the effects of the random geometry and the microphysical characteristics of cirrus clouds, on the averaged fluxes of solar radiation (in the visible wavelength range, as an example). In our work, we use a set of publicly accessible optical models, presented in detail in Section 2, and the Poisson model of broken clouds [22], making it possible to estimate the effect of stochastic cloud geometry on radiative characteristics in the wide range of variability in the shapes and sizes of ice crystals. We note that this model had already been used by ourselves before to estimate the effect of the random geometry of cirrus clouds on solar radiative transfer in the atmosphere; however, that simulation was carried out for a limited set of input parameters [22].

1. MODEL OF THE ATMOSPHERE AND CALCULATION TECHNIQUES

We consider the multilayer plane-parallel model of the atmosphere (0–100 km), one layer of which may be totally or partially occupied by cirrus clouds. A unit solar radiative flux is assumed to be incident at the top of the atmosphere; reflection from the underlying surface is described according to the Lambert law; molecular absorption is disregarded.

In this work, the simulated fluxes of solar radiation are analyzed in the visible wavelength range (wavelength $\lambda = 0.5 \text{ }\mu\text{m}$): (1) in the aerosol-molecular atmosphere, as well as in the presence of (2) overcast and (3) broken clouds. The first two cases are calculated using classical algorithms of the Monte Carlo method [23], implemented for the case of the multilayer horizontally homogeneous atmosphere (direct simulation, [24]). Averaged (over the set of cloud realizations) fluxes of solar radiation taking into account the effects of stochastic cloud geometry were calculated within the model on the basis of the Poisson point fluxes on the straight lines [22]. Clouds are approximated by rectangular parallelepipeds, elon-

gated in a single direction (bands), with the average horizontal sizes R_x and R_y (along the OX and OY axes, respectively) and height H . This shape is chosen from considerations that some cirrus clouds have the form of separate threadlike elements as white thin threads or slightly grayish elongated banks and patches, sometimes arranged into bands crossing the sky [25]. Cloud optical characteristics are assumed to be unchanged within all cloud elements, not varying from one realization to another. The model and examples of realizations of the cloud field were described in detail in [22]; a brief description can be found, e.g., in [26].

The method of closed equations (MCE, [22]), proposed by G.A. Titov, was used to calculate the average albedo $\langle A \rangle$ (at the TOA level) and diffuse transmission $\langle T_s \rangle$ (at the underlying surface). Within the cloud layer, the interaction of the optical radiation with the aerosol-molecular constituent of the atmosphere will be neglected.

The relative computation error did not exceed 0.5% in most cases.

2. INPUT PARAMETERS FOR THE RADIATION CALCULATIONS

2.1. Molecular-Aerosol Atmosphere

The aerosol model was specified in accordance with the Optical Properties of Aerosols and Clouds (OPAC, “continental average”) model [27]; the molecular scattering coefficients were calculated using the “midlatitude summer” meteorological model from [28]. Aerosol and Rayleigh scattering optical depths at $\lambda = 0.5 \text{ }\mu\text{m}$ were $\tau_a = 0.17$ and $\tau_R = 0.14$, respectively. The surface albedo was assumed to be equal to the albedo of grass cover A_s ($\lambda = 0.5 \text{ }\mu\text{m}$) = 0.045 [29].

2.2. Cirrus Clouds

Despite the fact that experimental data are difficult to obtain, abundant data on particle shape, ice content, and particle size distribution have been obtained over the past few decades, using lidar, aircraft, balloon-sonde, and satellite measurements in different regions of the globe. Based on these data, from the entire variety of particle shapes most common types of crystal habits have been identified in cirrus clouds (see, e.g., [30–33]): hexagonal (solid and hollow) columns, hexagonal plates, quasi-spherical particles (truncated spheres, i.e., droxtals, and prolate and oblate spheres), bullets (solid and hollow), rosettes (2D and 3D bullets), aggregates (structures of a few monocrystals, such as plates, columns, and bullets). The information on the shape of particles and their size distribution, as well as modern methods for calculating the optical characteristics of nonspherical particles under the assumption of their chaotic orientation, were used to compile the optical models of cirrus

Table 1. Cirrus cloud models

Model	Particle shape	Effective diameter, μm	Asymmetry factor $\langle\mu\rangle$ ($0.5\ \mu\text{m}$)
<i>BYH3 model (model number in given in parentheses in the order of increasing $\langle\mu\rangle$)</i>			
Aggregates of solid columns (ASC)	Aggregates of solid hexagonal columns	10	0.746 (1)
		30	0.749 (2)
		70	0.75 (3)
		120	0.75 (4)
General habit mixture (GHM)	Droxtals, plates, solid and hollow columns and bullets, aggregates of solid columns, large and small aggregates of plates	10	0.77 (5)
		30	0.783 (8)
		70	0.8 (10)
		120	0.811 (12)
Solid columns (SC)	Solid hexagonal columns	10	0.77 (6)
		30	0.782 (7)
		70	0.789 (9)
		120	0.804 (11)
<i>BYH2 model</i>			
Mixture of particles of different shapes	$D_{\text{max}} < 60\ \mu\text{m}$ – 100% droxtals;	10	0.777
	$60\ \mu\text{m} < D_{\text{max}} < 1000\ \mu\text{m}$ – 15% 3D bullets, 50% solid columns, 35% plates;	30	0.784
	$1000\ \mu\text{m} < D_{\text{max}} < 2500\ \mu\text{m}$ – 45% hollow columns, 45% solid columns, 10% aggregates;	70	0.81
	$2500\ \mu\text{m} < D_{\text{max}} < 9500\ \mu\text{m}$ – 97% 3D bullets, 3% aggregates	120	0.865
<i>OPAC model</i>			
Cirrus1, temperature of -25°C	Hexagonal columns	183.4	0.783
Cirrus2, temperature of -50°C	Rosettes of hexagonal columns	114.8	0.77
Cirrus3, temperature of -50°C	Cirrus2 model with addition of small particles	68.6	0.763

clouds, which had been widely used to solve the problems of remote sensing (retrieval of cloud parameters on the basis of radiometric observations) and interpret the measurements of reflected radiation [15, 34–40].

Table 1 presents 19 cirrus cloud models used in this work: two model versions developed by Baum, Yang, Heymsfield et al., [31, 41, 42] (henceforth, BYH2 (4 variants) and BYH3 (12 variants), i.e., the second and third versions, respectively) and cirrus cloud models, presented in OPAC package (3 variants) [27].

The BYH2 and BYH3 optical characteristics were calculated for microstructure models, differing both in the particle shape and size distribution, characterized by the effective diameter D_{eff} . The BYH3 model [42] is an improved and complemented version of the BYH2 model [31, 41]: it has a much wider spectral range and includes three types of particle surface roughness, three types of particle mixtures as functions of particle shape and size, total scattering matrix for particles

with a strong roughness, a finer grid over the scattering angle of the scattering phase function, etc. The BYH2 and BYH3 optical characteristics strongly differ because surface roughness, accounted for in the BYH3 model, levels off the angular behavior of the scattering phase function and, in contrast to smooth particles, leads to a less pronounced halo and much weaker backscattering [35].

The BYH3 model was tested through comparison with experimental data (see, e.g., [42] and bibliography therein). In situ observations were used to show that the ice water content IWC and the diameter of the mean mass D_{mm} best agreed for the model, specifying the particles shaped as solid columns (SC model); while the PARASOL-measured reflectivity of clouds was the closest to the simulations for the mixture of particles of different shapes with strong surface roughness (GHM model). The optimal correspondence between COT values, retrieved on the basis of measurements in the solar and IR wavelength ranges, was

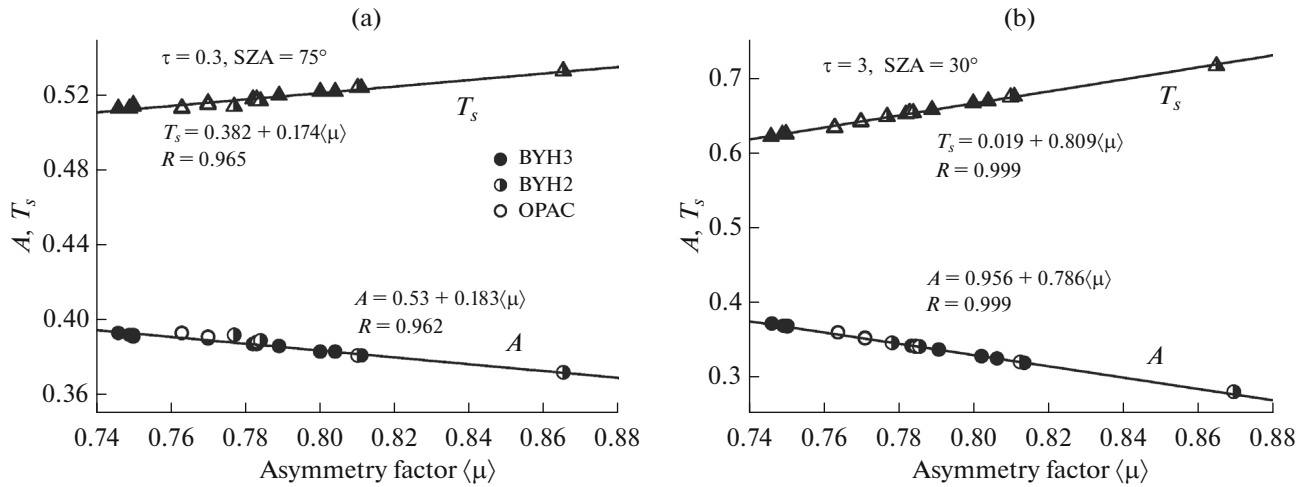


Fig. 1. Albedo A and diffuse transmission T_s of overcast cirrus clouds versus particle shape and sizes (Table 1) for different τ and SZA.

observed when using a model comprising aggregates of solid columns (ASC). We conclude by noting that the BYH2 and BYH3 models were used as a basis for the cirrus cloud models, which were used and are being used now to develop remote sensing products on the basis of MODIS measurements: BYH2, collection 5, and BYH3 (model of aggregates of solid columns), collection 6 [34, 35].

As already indicated above, the radiation calculations, in addition to BYH2 and BYH3 models, will also use OPAC models, the optical characteristics of which correspond to three different microstructure models (Cirrus1, Cirrus2, and Cirrus3), depending on cloud temperature and particle shape [27]. Pronounced halos at the scattering angles $\theta_1 \approx 22^\circ$ and $\theta_2 \approx 46^\circ$ are present in the visible range due to the hexagonal shape and smooth surface of ice particles. Angular structures of the scattering phase function in the BYH3 and OPAC models were compared before in [43]. We also note that the asymmetry factor (mean cosine of the scattering phase function) $\langle\mu\rangle$ for 18 out of 19 crystal models, considered here, varies in the range 0.746–0.811, i.e., for all but BYH2 model ($D_{\text{eff}} = 120 \mu\text{m}$), for which $\langle\mu\rangle = 0.865$.

The radiative transfer simulation is performed in the presence of overcast and broken cirrus clouds for optically thin (optical thickness $\tau = 0.3$) and optically dense ($\tau = 3$) clouds [44] occupying the layer of 9–10 km; cloud single scattering albedo was set to 1.

The illumination conditions were specified in terms of the solar zenith angle $\text{SZA} = \{30^\circ, 75^\circ\}$ and solar azimuth angle SAA, counted off from the positive direction of the OX axis, and was set to 0 in all calculations. In the general case, the SAA can be chosen to be arbitrary, $0^\circ \leq \text{SAA} \leq 180^\circ$, which for fixed horizontal extents of the bands R_x and R_y , makes it possible to study how the average radiative fluxes change as functions of illumination conditions. In this work, we restrict ourselves to the consideration of two extreme

cases, where the direct solar radiation is incident along and across the bands: in this case, it is sufficient to fix $\text{SAA} = 0$ and change the horizontal extents of the bands along the OX and OY axes. The mean horizontal extents of clouds were chosen to be $R_x = 10 \text{ km}$, $R_y = 1 \text{ km}$ and $R_x = 1 \text{ km}$, $R_y = 10 \text{ km}$. The direct solar radiation propagates along (across) elongated bands in the first (second) case.

3. RESULTS OF NUMERICAL EXPERIMENTS

This section presents the results of numerical simulation of the albedo A and diffuse transmission T_s of the atmosphere at the TOA and underlying surface, respectively, and estimates, on their basis, (1) the effect of microstructure in overcast horizontally homogeneous clouds (subsection 3.1), and (2) the effects of the random geometry for a fixed optical model of cirrus clouds (subsection 3.2), as well as discussion of the joint influence of the microstructure and 3D effects of clouds on the formation of scattered fluxes of solar radiation in broken cirrus clouds on the set of the BYH3 models (subsection 3.3). In this work, we do not consider the fluxes of direct radiation at the underlying surface; this is because the effect of the cloud microstructure is estimated for a fixed optical thickness and, as such, does not depend on the particle shape and size spectrum, and is determined only by the effects of stochastic geometry.

3.1. Effect of Cirrus Cloud Microstructure (Overcast Horizontally Homogeneous Clouds)

Figure 1 presents the albedo A and diffuse transmission T_s , calculated using 19 cirrus cloud models, presented in Table 1. The calculations show that A and T_s weakly vary as the angular structure of the scattering phase function changes (absence/presence of halo, elongation degree of the scattering phase function

around “forward” direction, etc.) and are determined mainly by the asymmetry factor $\langle\mu\rangle$. In addition, the dependences of A and T_s on $\langle\mu\rangle$ for fixed COT and SZA are close to linear and characterized by a high correlation coefficient ($R > 0.96$). Considering that the mean cosine varies in the range 0.746–0.811 in all but the BYH2 model ($D_{\text{eff}} = 120 \mu\text{m}$), the flux calculations using the BYH3 model (number of variants $N_{Ci} = 12$) will be considered below because they totally reflect the A and T_s variations on the set of cirrus cloud models presented in Table 1.

Obviously, the quality of the radiation calculations (in particular, when compared to experimental data) depends on how accurate is the information in the cloud optical model. Next, we will consider two situations: suppose that (1) we know only the cloud optical thickness τ , and (2) in addition to τ , data on the effective size of ice crystals D_{eff} are available.

In the first case, an important aspect is the relationship between the optical thicknesses of the clear-sky atmosphere $\tau_{\text{clr}} = \tau_a + \tau_R$ and cirrus clouds τ , which can either be less than or comparable to τ_{clr} . This factor will be estimated by comparing the variability ranges of albedo and diffuse transmission, calculated taking into account the aerosol-molecular constituent of the atmosphere (A and T_s), with analogous calculations performed for an isolated cloud layer (A_{Ci} and $T_{s,Ci}$). In the latter case, the variations in albedo and diffuse transmission depend exclusively on the optical model of cirrus clouds.

The variability range of $F = A, T_s, A_{Ci}, T_{s,Ci}$ will be defined by the minimal and maximal values of their relative differences $\delta_j^i F$, $i, j = 1, \dots, N_{Ci} = 12$, arising due to the use of different BYH3 models in the calculations:

$$\Delta^i F = \left\{ \min_j \delta_j^i F, \max_j \delta_j^i F \right\}, \quad (1)$$

$$\delta_j^i F = 100\% \times (F^j - F^i) / F^i, \quad i, j = 1, \dots, 12.$$

Analysis of results from numerical simulation shows the following things. If τ is smaller than or comparable to τ_{clr} , the differences, determined by the specific features of the ice crystal model, are appreciably smoothed out. For instance, when $\tau \approx \tau_{\text{clr}} \approx 0.3$ (Figs. 2a and 2b), the range of the differences in albedo and diffuse transmission between the isolated layer and the cloudy atmosphere decreases from $\sim \pm 12$ to $\sim \pm 2\%$ and from $\sim \pm 5$ to $\sim \pm 2\%$, respectively, depending on the model. As the optical thickness of cirrus clouds increases while τ_{clr} remains unchanged, the effect of aerosol attenuation and molecular scattering weakens: when $\tau = 3$, the differences between $\Delta^i A_{Ci}$ and $\Delta^i A$ decrease insignificantly (from ± 20 to $\pm 15\%$), while $\Delta^i T_{s,Ci}$ and $\Delta^i T_s$ differ little ($\pm 10\%$) (Figs. 2c and 2d). As follows from the results presented, the greater the difference in the corresponding asymmetry factors, the

larger the relative differences in the average fluxes, caused by the variations in optical models; while in the cloudy atmosphere, as compared to the isolated layer, the greater the COT for typical values $0.3 \leq \tau \leq 3$, the stronger the dependence of albedo and diffuse transmission on the model. In addition, fluxes of reflected radiation are more sensitive to the variations in the microstructure.

We will estimate how ice crystal shape influences the albedo and diffuse transmission at a fixed effective particle diameter. Simulations show (Fig. 3) that the particle shape effect depends on the COT and increases with D_{eff} . For instance, when $\tau = 3$, the uncertainty in the A and T_s calculations due to the absence of information on crystal shape increases from $\sim \pm 5$ to $\sim \pm 15\%$ and from $\sim \pm 3$ to $\sim \pm 8\%$, respectively, as D_{eff} increases from 10 to 120 μm . In the optically thin cirrus clouds ($\tau = 0.3$), the particle shape effect is much weaker, not exceeding 2–3% in the entire range $10 \mu\text{m} \leq D_{\text{eff}} \leq 120 \mu\text{m}$ considered here.

We conclude this subsection by noting that: from comparison of Figs. 2 and 3 it follows that the main factors, on which the uncertainty in the flux calculations depends, are the cloud optical thickness and particle shape. Analogous results were also obtained in [18, 44]; however, those findings indicate that the effect crystal size on the radiative fluxes increases in the presence of absorption.

3.2. Estimate of the Effect of Horizontal Inhomogeneity of Cirrus Clouds

To understand how the random cloud geometry influences the average fluxes $\langle F \rangle = \{ \langle A \rangle, \langle T_s \rangle \}$, we choose the GHM model ($D_{\text{eff}} = 70 \mu\text{m}$) and estimate the quantities

$$\Delta_{3D} F = 100\% \times (F_{\text{o-c}} - \langle F \rangle) / \langle F \rangle, \quad (2)$$

$$F_{\text{o-c}} = (1 - CF) \times F_{\text{clr}} + CF \times F,$$

where $F_{\text{o-c}}$ is the solar radiative flux, calculated by simulating fluxes under the conditions of clear sky F_{clr} and overcast clouds F (“open–closed” approximation [22, 46]); and CF is the cloud fraction in fractions of unity. This approximation is used to describe the radiative characteristics in clouds, the vertical dimensions of which are much smaller than the horizontal (stratus clouds).

We will consider two different situations, associated with the orientation of cloud bands: (1) $R_x = 10 \text{ km}$, $R_y = 1 \text{ km}$ (Fig. 4a) and (2) $R_x = 1 \text{ km}$, $R_y = 10 \text{ km}$ (Fig. 4b). For the analysis, we choose situations with optically dense cirrus clouds ($\tau = 3$), because with growing COT, the relative role of cloud sides and the radiation interaction of individual clouds increase, and 3D cloud effects become more pronounced [22].

If the solar zenith angle is close to the zenith (SZA = 30°), the inequality $\langle A \rangle < A_{\text{o-c}}$ holds indepen-

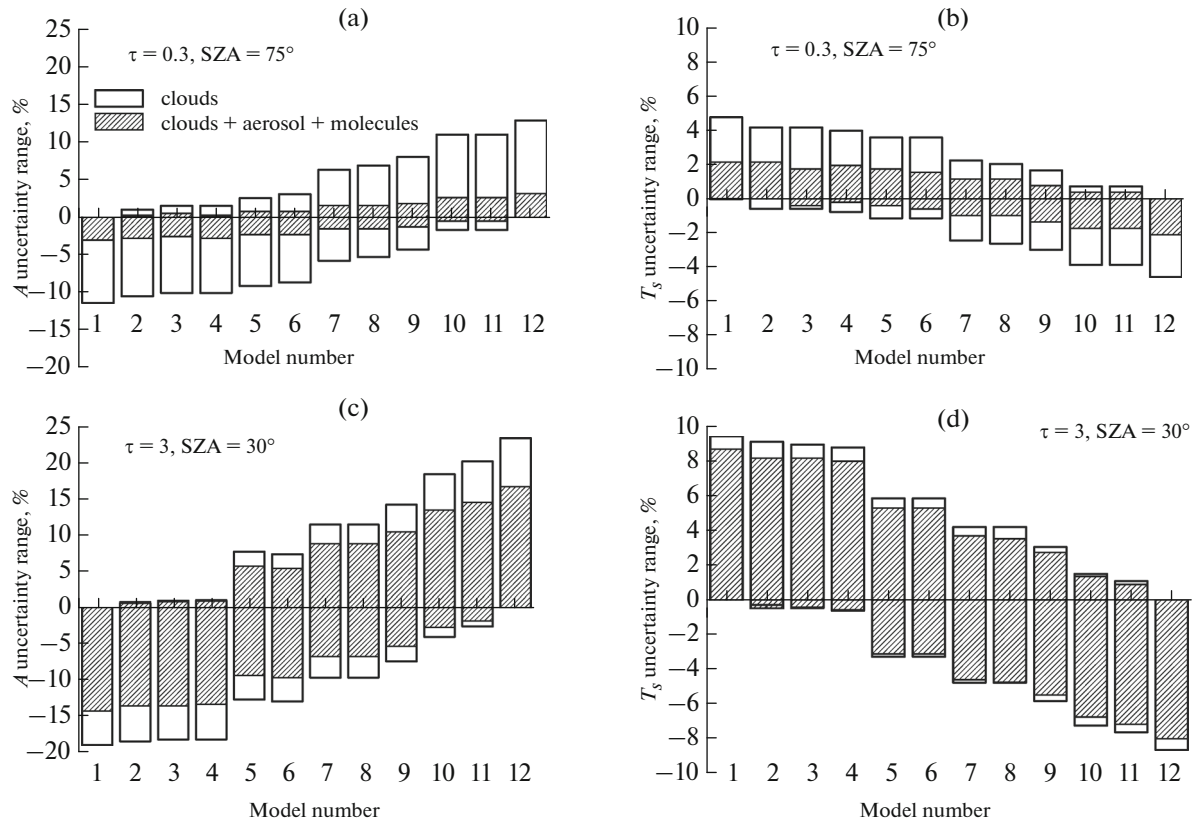


Fig. 2. Variability ranges of (a, c) A and (b, d) T_s with variations in optical models of cirrus clouds, entering BYH3, for different τ and SZA.

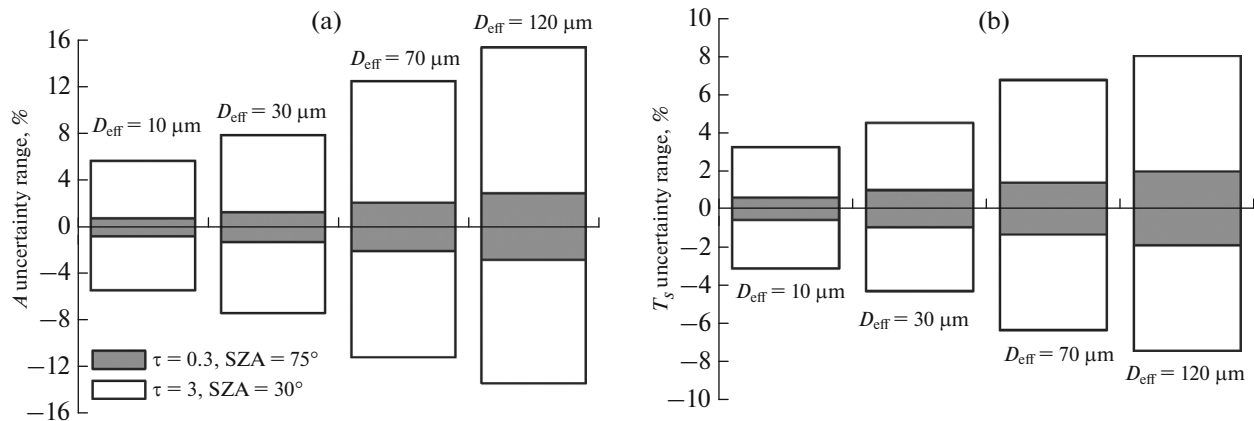


Fig. 3. Dependence of the (a) A and (b) T_s variations on the shape for fixed effective particle diameter D_{eff} and different τ and SZA.

dent of the orientation of cloud bands (Fig. 5, left). This is because the fraction of direct radiation weakly depends on the cloud field structure for such illumination conditions; and the formula $\langle A \rangle + \langle T_s \rangle \approx A_{o-c} + T_{s,o-c}$ holds for scattered radiation in the case of conservative scattering and small A_s values. Almost all radiation leaves through cloud tops and bottoms in the case of stratus clouds (“open–closed” approximation); while in the field, consisting of finite-extent clouds, a considerable

part of the radiation may leave through the cloud sides, experiencing, on average, fewer scattering events than radiation leaving through the cloud top and bottom. Since the scattering phase function is strongly elongated in the “forward” direction, radiation leaving through the cloud sides mostly contributes to transmission, i.e., $\langle T_s \rangle > T_{s,o-c}$ and, hence, $\langle A \rangle < A_{o-c}$.

For large solar zenith angles (SZA = 75°) the relationship between $\langle A \rangle$ and A_{o-c} depends on the cloud

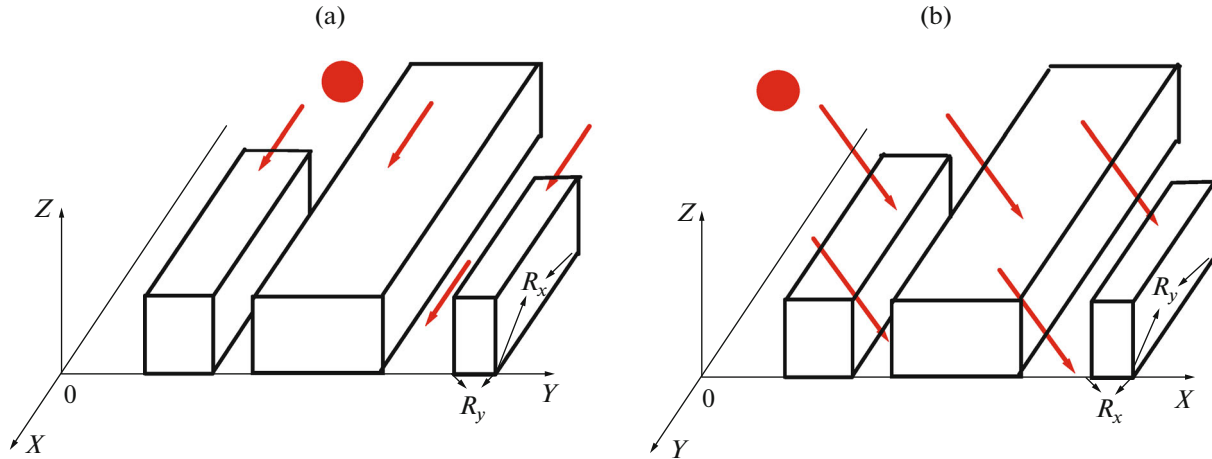


Fig. 4. Schematic illustration of arrangement of cloud field as a function of orientation of bands for different illumination conditions: direct solar radiation is incident (a) along and (b) across the bands.

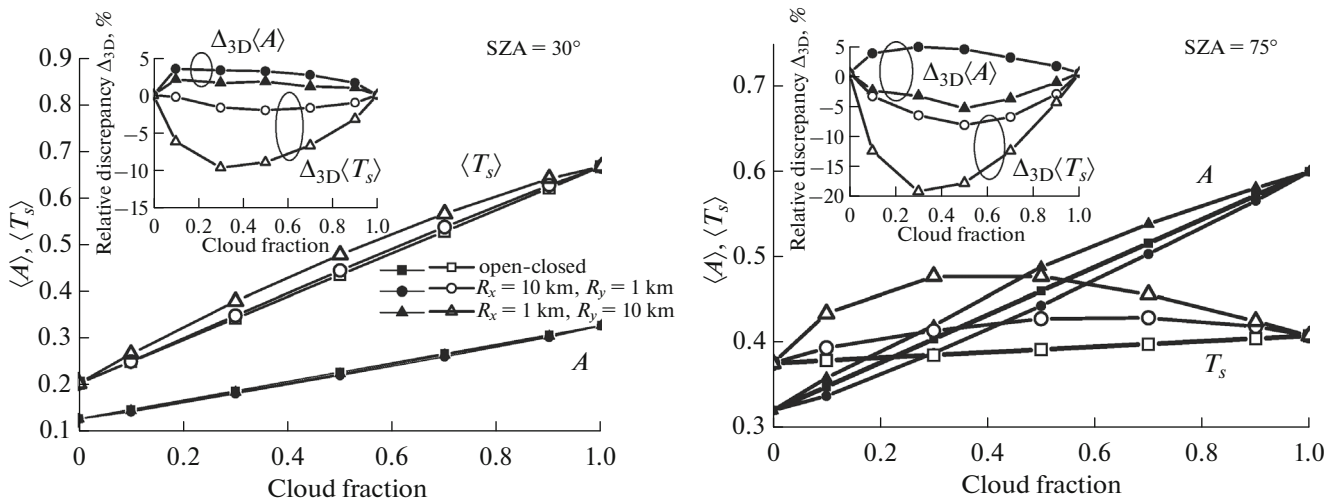


Fig. 5. Dependences of the average albedo and diffuse transmission calculated with and without accounting for the horizontal cloud inhomogeneity and of their average discrepancies on the cloud fraction for different SZAs; GHM model ($D_{\text{eff}} = 70 \mu\text{m}$), $\tau = 3$.

orientation relative to the direction of incident solar radiation. If solar radiation is incident *along* elongated bands ($R_x = 10 \text{ km}, R_y = 1 \text{ km}$), the role of cloud sides is comparatively minor, and so we can assume that

$$\langle A(R_x = 10 \text{ km}, R_y = 1 \text{ km}) \rangle + \langle T_s(R_x = 10 \text{ km}, R_y = 1 \text{ km}) \rangle \approx A_{o-c} + T_{s,o-c}. \quad (3)$$

As for $\text{SZA} = 30^\circ$, this leads to the inequalities

$$\langle T_s(R_x = 10 \text{ km}, R_y = 1 \text{ km}) \rangle > T_{s,o-c} \quad (4)$$

and $\langle A(R_x = 10 \text{ km}, R_y = 1 \text{ km}) \rangle < A_{o-c}$.

If the radiation is incident *across* the bands (Fig. 4b), cloud sides screen the direction “toward the Sun,” and the contribution of scattered radiation increases in view of a much smaller fraction of direct radiation, i.e.,

$$\langle A(R_x = 1 \text{ km}, R_y = 10 \text{ km}) \rangle + \langle T_s(R_x = 1 \text{ km}, R_y = 10 \text{ km}) \rangle > A_{o-c} + T_{s,o-c}. \quad (5)$$

For these parameters of the problem this inequality is so strong that, in addition to the relationship

$$\langle T_s(R_x = 1 \text{ km}, R_y = 10 \text{ km}) \rangle > T_{s,o-c}, \quad (6)$$

the analogous inequality also holds for the albedo, namely

$$\langle A(R_x = 1 \text{ km}, R_y = 10 \text{ km}) \rangle > A_{o-c}. \quad (7)$$

These quantitative estimates of the random geometry effects show (Fig. 5) that the deviations due to the open–closed approximation are maximal for the fluxes of diffuse transmission: at $CF = 0.3\text{--}0.5$ the $\Delta_{3D}\langle T_s \rangle$ value varies from ~ -10 to -20% , depending

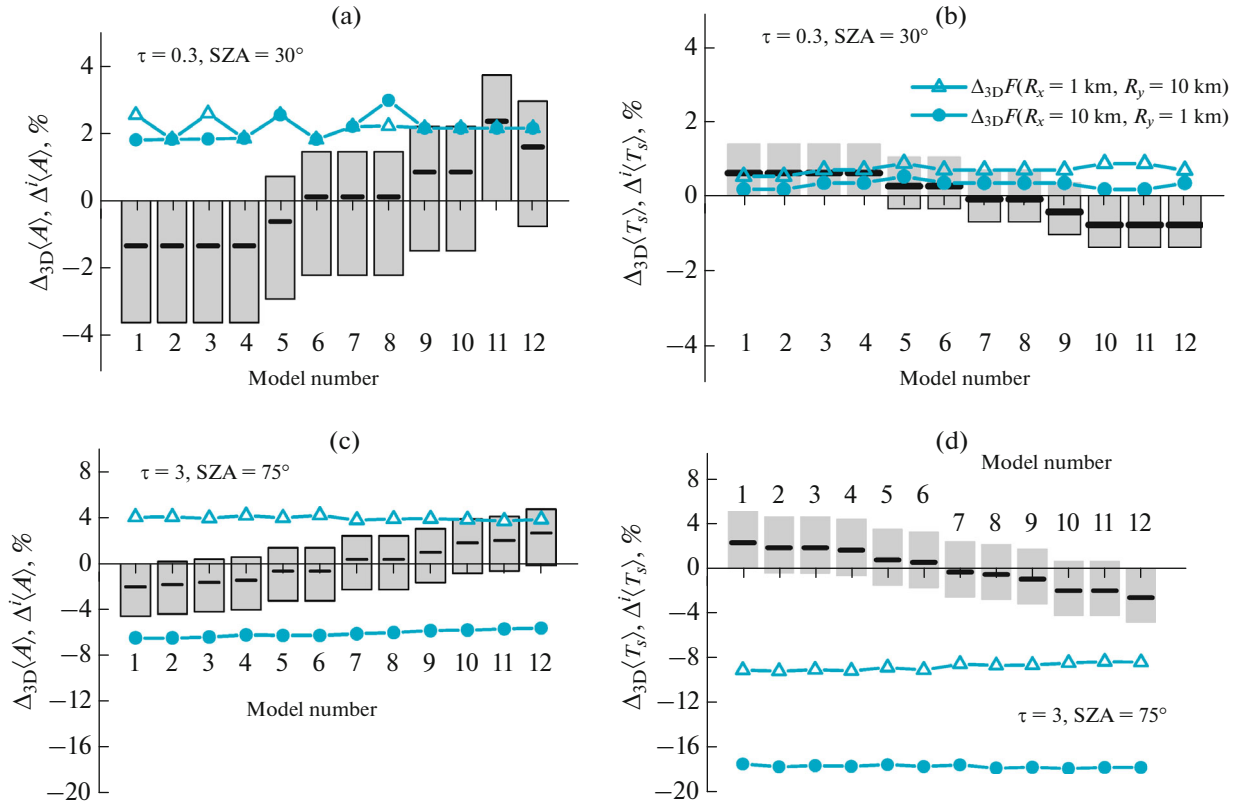


Fig. 6. Uncertainties of simulating (a, c) the average albedo and (b, d) diffuse transmission due to the absence of information on cloud microstructure and to the neglect of the random geometry effects at $CF = 0.5$. Gray columns indicate the $\langle A \rangle$ and $\langle T_s \rangle$ variability ranges with variations in the cirrus cloud microstructure; horizontal lines indicate the average uncertainties; blue lines indicate the errors due to the neglect of the horizontal inhomogeneity of the cloud layer.

on the SZA and direction of the cloud bands. The effect of the cloud random geometry on the mean albedo is weaker, not going beyond the interval from 2 (SZA = 30°) to 5% (SZA = 75°) in absolute value. For small optical thicknesses ($\tau = 0.3$) the effect of the random geometry on $\langle A \rangle$ and $\langle T_s \rangle$ is less significant, being within 1–3% in absolute value.

3.3. Joint Effect of Microstructure and Stochastic Geometry on Average Solar Radiative Fluxes

We will consider the relationship between the uncertainties in the albedo and diffuse transmission calculations due to (1) the absence of information on the microstructure of cirrus clouds $\Delta^i \langle F \rangle$ and (2) the neglect of the effects of random geometry within a known ice crystal model $\Delta_{3D} \langle F^i \rangle$, $i = 1, \dots, N_{Ci}$. Preliminary calculations showed that the variability range of the average fluxes due to variations in ice crystal shape and sizes barely depends on the orientation of cloud bands relative to the incident radiation; therefore, $\Delta^i \langle F \rangle$ will be estimated by simulating mean radiative fluxes for $R_x = 1$ km, $R_y = 10$ km.

Analysis of the differences in the average fluxes among the entire set of the optical models $i = 1, \dots, N_{Ci}$

shows that the variability range $\Delta^i \langle F \rangle$ does not exceed 4–5% in absolute value, the average being $\pm 2\%$, for the moderate cloud fractions $CF = 0.5$ in the parameter variability range considered here (Fig. 6). The microstructure effect is less somewhat in broken than overcast clouds (Figs. 2 and 6). For instance, $\Delta^i \langle F \rangle$, $i = 1, \dots, N_{Ci}$ decreases not as significantly (mainly by 1–2%) at $\tau = 0.3$; while at $\tau = 3$ and SZA = 75°, $\Delta^i \langle T_s \rangle$ decreases by almost a factor of two: from (–6%, +10%) to (–4%, +5%) for a relatively small change in $\Delta^i \langle A \rangle$ (by ~ 1 –2%).

In the optically thin clouds, the average value of uncertainty due to the absence of data on the crystal shape and sizes $\Delta^i \langle F \rangle$ is comparable to $\Delta_{3D} F^i$, $i = 1, \dots, N_{Ci}$ due to the use of horizontally homogeneous model in the calculations, and is within 2% in absolute value (Figs. 6a and 6b). As the COT increases to $\tau = 3$ at SZA = 75°, the cloud random geometry effect increases: the neglect of the horizontal inhomogeneity in albedo and diffuse transmission calculations leads to uncertainties in the ranges (–6%, 4%) and (–20%, –10%), respectively, the average value of $\Delta^i \langle F \rangle$ being $\pm 2\%$. We stress that, while $\langle T_s^i \rangle$ is underestimated in the simulation of diffuse transmission in the

open–closed approximation, the average albedo calculations may either overestimate or underestimate this characteristic (causes for this were discussed in subsection 3.2; see also Fig. 5).

CONCLUSIONS

In this work we consider the results from statistical simulation of albedo A and diffuse transmission T_s at the TOA and underlying surface in cirrus clouds (visible range), with the purpose of comparing how they are influenced by two factors, i.e., cloud microstructure and stochastic geometry.

The second and third versions of the model, suggested by Baum et al. (BYH2 and BYH3), as well as cirrus cloud models available from OPAC model, were used to study the effect of the shape and sizes of chaotically oriented ice crystals. Analysis of the microstructure effect in *overcast* horizontally homogeneous clouds with the optical thickness $0.3 \leq \tau \leq 3$, performed at the first stage, showed that the scattered radiative fluxes weakly depend on the angular structure of the scattering phase functions, and are determined mainly by the asymmetry factor. The estimate of relative differences in radiative fluxes, calculated using the BYH3 model (12 variants, depending on the particle shape and effective diameter), showed that the microstructure effect increases with COT: when $\tau = 3$, the ranges of uncertainties due to the absence of information on particle shape and sizes are $\sim \pm 15$ and $\sim \pm 10\%$ in the A and T_s calculations, respectively. As D_{eff} increases from 10 to 120 μm , the crystal shape effect intensifies, and the range of relative differences changes from $\sim \pm 5$ to $\sim \pm 15\%$ for A and from $\sim \pm 3$ to $\sim \pm 8\%$ for T_s . In optically thin cirrus clouds with $\tau = 0.3$, the shape effect on the A and T_s calculations is much weaker and does not exceed 2–3% in absolute value.

Estimate of how the stochastic cloud geometry influences the average fluxes of solar radiation is obtained by comparing calculations in the Poisson model of broken clouds in the open–closed approximation using one of BYH3 variants as an example. It is shown that the random geometry effect, which is maximal for moderate cloud fractions $CF = 0.3\text{--}0.5$ and $\tau = 3$, depends on the orientation of elongated clouds relative to the incident solar radiation and is manifested most strongly for large solar zenith angles: the average albedo can either be overestimated or underestimated within 5%, while the average diffuse transmission is underestimated within 10–20%.

The joint effect of the random geometry and microstructure of cirrus clouds on the entire set of the BYH3 model variants, considered here, is analyzed for moderate cloud fractions ($CF = 0.5$). It is shown that the average uncertainty due to the absence of information on the microstructure is within $\sim \pm 2\%$. This uncertainty is comparable to the random geometry

effects in optically thin clouds ($<1\text{--}2\%$), while in optically dense clouds the range of errors due to the neglect of cloud horizontal inhomogeneity increases, being (–6%, 4%) and (–10%, –20%) in albedo and diffuse transmission calculations, respectively.

FUNDING

A modification of the statistical simulation algorithm for solar radiative transfer in broken cirrus clouds and preparation of input parameters were supported by the Ministry of Science and Higher Education of the Russian Federation (V.E. Zuev Institute of Atmospheric Optics, Siberian Branch, Russian Academy of Sciences); numerical experiments and analysis of results were supported by the Russian Foundation for Basic Research (grant no. 19-01-00351).

CONFLICT OF INTEREST

The authors declare that they have no conflicts of interest.

REFERENCES

1. K. N. Liou, “Influence of cirrus clouds on weather and climate processes—a global perspective,” *Mon. Weather. Rev.* **114**, 1167–1199 (1986).
2. A. J. Baran, “From the single-scattering properties of ice crystals to climate prediction: A way forward,” *Atmos. Res.* **112**, 45–69 (2012).
3. M. H. Zhang, W. Y. Lin, S. A. Klein, J. T. Bacmeister, S. Bony, R. T. Cederwall, A. D. Del Genio, J. J. Hack, N. G. Loeb, U. Lohmann, P. Minnis, I. Musat, R. Pincus, P. Stier, M. J. Suarez, M. J. Webb, J. B. Wu, S. C. Xie, M.-S. Yao, and J. H. Zhang, “Comparing clouds and their seasonal variations in 10 atmospheric general circulation models with satellite measurements,” *J. Geophys. Res.* **110**, D15S02 (2005).
4. N. G. Loeb and J. A. Coakley, “Inference of marine stratus cloud optical depths from satellite measurements: Does 1D theory apply?,” *J. Clim.* **11** (2), 215–233 (1998).
5. T. Varnai and A. Marshak, “Statistical analysis of the uncertainties in cloud optical depth retrievals caused by three-dimensional radiative effects,” *J. Atmos. Sci.* **58** (12), 1540–1548 (2001).
6. H. Iwabuchi and T. Hayasaka, “Effects of cloud horizontal inhomogeneity on the optical thickness retrieved from moderate-resolution satellite data,” *J. Atmos. Sci.* **59** (14), 2227–2242 (2002).
7. T. Zinner and B. Mayer, “Remote sensing of stratocumulus clouds: Uncertainties and biases due to inhomogeneity,” *J. Geophys. Res.* **111**, D14209 (2006).
8. A. Marshak, S. Platnick, T. Varnai, G. Wen, and R. F. Cahalan, “Impact of 3D Radiative effects on satellite retrievals of cloud droplet sizes,” *J. Geophys. Res.* **111**, D09207 (2006).
9. C. Cornet and R. Davies, “Use of MISR measurements to study the radiative transfer of an isolated convective cloud: Implications for cloud optical thickness retrieval,” *J. Geophys. Res.* **113**, D04202 (2008).

10. Y. Zhou, X. Sun, R. Zhang, C. Zhang, H. Li, J. Zhou, and S. Li, "Influences of cloud heterogeneity on cirrus optical properties retrieved from the visible and near-infrared channels of MODIS/SEVIRI for flat and optically thick cirrus clouds," *J. Quant. Spectrosc. Radiat. Transfer* **187**, 232–246 (2017).
11. T. Fauchez, S. Platnick, T. Varnai, K. Meyer, C. Cornet, and F. Szczap, "Scale dependence of cirrus heterogeneity effects. Part II: MODIS NIR and SWIR channels," *Atmos. Chem. Phys.* **18**, 12105–12121 (2018).
12. H. Kalesse, Ph.D. Thesis (Johannes Gutenberg University, Mainz, Germany, 2009), p. 65–85.
13. T. Chen, W. B. Rossow, and Y. Zhang, "Radiative effects of cloud-type variations," *J. Clim.* **13** (1), 264–286 (2000).
14. Y. Zhang, A. Macke, and F. Albers, "Effect of crystal size spectrum and crystal shape on stratiform cirrus radiative forcing," *Atmos. Res.* **52**, 59–75 (1999).
15. N. G. Loeb, P. Yang, F. G. Rose, G. Hong, S. Sun-Mack, P. Minnis, S. Kato, S.-H. Ham, W. L. Jr. Smith, S. Hioki, and G. Tang, "Impact of ice cloud microphysics on satellite cloud retrievals and broadband flux radiative transfer model calculations," *J. Clim.* **31** (5), 1851–1864 (2018).
16. N. Buschmann, G. M. McFarquhar, and A. J. Heymsfield, "Effects of observed horizontal inhomogeneities within cirrus clouds on solar radiative transfer," *J. Geophys. Res. D* **107** (20), 4445 (2002).
17. B. Carlin, Q. Fu, U. Lohmann, G. G. Mace, K. Sassen, and J. M. Comstock, "High-cloud horizontal inhomogeneity and solar albedo bias," *J. Clim.* **15** (17), 2321–2339 (2002).
18. I. Schlimme, A. Macke, and J. Reichardt, "The impact of ice crystal shapes, size distributions, and spatial structures of cirrus clouds on solar radiative fluxes," *J. Atmos. Sci.* **62** (7), 2274–2283 (2005).
19. F. Szczap, Y. Gour, T. Fauchez, C. Cornet, T. Faure, O. Jourdan, G. Penide, and P. Dubuisson, "A flexible three-dimensional stratocumulus, cumulus and cirrus cloud generator (3DCLOUD) based on drastically simplified atmospheric equations and the Fourier transform framework," *Geosci. Model Dev.* **7**, 1779–1801 (2014).
20. M. Schafer, E. Bierwirth, A. Ehrlich, E. Jakel, F. Werner, and M. Wendisch, "Directional, horizontal inhomogeneities of cloud optical thickness fields retrieved from ground-based and airborne spectral imaging," *Atmos. Chem. Phys.* **17**, 2359–2372 (2017).
21. T. Fauchez, S. Platnick, K. Meyer, C. Cornet, F. Szczap, and T. Varnai, "Scale dependence of cirrus horizontal heterogeneity effects on TOA measurements—Part I: MODIS brightness temperatures in the thermal infrared," *Atmos. Chem. Phys.* **17**, 8489–8508 (2017).
22. V. E. Zuev and G. A. Titov, *Atmospheric Optics and Climate* (Spektr, Tomsk, 1996) [in Russian].
23. G. I. Marchuk, G. A. Mikhailov, M. A. Nazarialiev, R. A. Darbinyan, B. A. Kargin, and B. S. Elepov, *Monte Carlo Method in Atmospheric Optics* (Nauka, Novosibirsk, 1976) [in Russian].
24. T. B. Zhuravleva, "Simulation of solar radiative transfer under different atmospheric conditions. Part I. The deterministic atmosphere," *Atmos. Ocean. Opt.* **21** (2), 81–95 (2008).
25. *Clouds and Cloudy Atmosphere. Handbook*, Ed. by I. P. Mazin and A. Kh. Khrgian (Gidrometeoizdat, Leningrad, 1989) [in Russian].
26. S. M. Prigarin, T. B. Zhuravleva, and P. V. Volikova, "Poisson model of multilayer broken clouds," *Atmos. Ocean. Opt.* **15** (10), 832–838 (2002).
27. M. Hess, P. Koepke, and I. Schult, "Optical properties of aerosols and clouds: The software package OPAC," *Bull. Amer. Meteor. Soc.* **79**, 831–844 (1998).
28. F. X. Kneizys, D. S. Robertson, L. W. Abreu, P. Acharya, G. P. Anderson, L. S. Rothman, J. H. Chetwynd, J. E. A. Selby, E. P. Shettle, W. O. Gallery, A. Berk, S. A. Clough, and L. S. Bernstein, *The MODTRAN 2/3 Report and LOWTRAN 7 Model* (Phillips Laboratory, Geophysics Directorate, Hanscom, MA, 1996).
29. S. J. Hook, *ASTER Spectral Library: Johns Hopkins University (JHU) spectral library; Jet Propulsion Laboratory (JPL) spectral library; The United States Geological Survey (USGS-Reston) spectral library*. Dedicated CD-ROM. Version 1.2. (1998).
30. I. P. Mazin and S. M. Shmeter, *Clouds, Structure, and Physics of Formation* (Gidrometeoizdat, Leningrad, 1983) [in Russian].
31. B. A. Baum, A. J. Heymsfield, P. Yang, and S. T. Bedka, "Bulk scattering models for the remote sensing of ice clouds. Part 1: Microphysical data and models," *J. Appl. Meteorol.* **44** (12), 1885–1895 (2005).
32. A. J. Heymsfield, C. Schmitt, and A. Bansemmer, "Ice cloud particle size distributions and pressure dependent terminal velocities from in situ observations at temperatures from 0° to –86°C," *J. Atmos. Sci.* **70**, 4123–4154 (2013).
33. A. M. Fridlind, R. Atlas, B. van Dierenhoven, J. Um, G. M. McFarquhar, A. S. Ackerman, E. J. Moyer, and R. P. Lawson, "Derivation of physical and optical properties of mid-latitude cirrus ice crystals for a size-resolved cloud microphysics model," *Atmos. Chem. Phys.* **16**, 7251–7283 (2016).
34. S. Platnick, K. G. Meyer, M. D. King, G. Wind, N. Amarasinghe, B. Marchant, G. T. Arnold, Z. Zhang, P. A. Hubanks, R. E. Holz, P. Yang, W. L. Ridgway, and J. Riedi, "The MODIS cloud optical and microphysical products: collection 6 updates and examples from Terra and Aqua," *IEEE Trans. Geosci. Rem. Sens.* **55** (1), 502–525 (2017).
35. P. Yang, S. Hioki, M. Saito, C.-P. Kuo, B. Baum, and K.-N. Liou, "A review of ice cloud optical property models for passive satellite remote sensing," *Atmosphere* **9** (12), 499 (2018).
36. P. Minnis, S. Sun-Mack, D. F. Young, P. W. Heck, D. P. Garber, Y. Chen, D. A. Spangenberg, R. F. Arduini, Q. Z. Trepte, Jr. Smith, J. K. Ayers, S. C. Gibson, W. F. Miller, G. Hong, V. Chakrapani, Y. Takano, K.-N. Liou, Y. Xie, and P. Yang, "CERES edition-2 cloud property retrievals using TRMM VIRS and Terra and Aqua MODIS data, Part I: Algorithms," *IEEE Trans. Geosci. Remote Sens.* **49**, 4374–4400 (2011).
37. Z. Zhang, P. Yang, G. W. Kattawar, J. Riedi, C.-L. Labonnote, B. A. Baum, S. Platnick, and H.-L. Huang, "Influence of ice particle model on satellite ice cloud

- retrieval: Lessons learned from MODIS and POLDER cloud product comparison,” *Atmos. Chem. Phys.* **9**, 7115–7129 (2009).
38. C.-L. Labonnote, G. Brogniez, J. C. Buriez, and M. Doutriaux-Boucher, “Polarized light scattering by inhomogeneous hexagonal monocrystals: Validation with ADEOS-POLDER measurements,” *J. Geophys. Res.* **106**, 12139–12153 (2001).
 39. B. H. Cole, P. Yang, B. A. Baum, J. Riedi, C.-L. Labonnote, F. Thieuleux, and S. Platnick, “Comparison of PARASOL observations with polarized reflectances simulated using different ice habit mixtures,” *J. Appl. Meteor. Climatol.* **52**, 186–196 (2013).
 40. B. H. Cole, P. Yang, B. A. Baum, J. Riedi, and C.-L. Labonnote, “Ice particle habit and surface roughness derived from PARASOL polarization measurements,” *Atmos. Chem. Phys.* **14**, 3739–3750 (2014).
 41. B. A. Baum, P. Yang, A. J. Heymsfield, S. Platnick, M. D. King, Y.-X. Hu, and S. T. Bedka, “Bulk scattering properties for the remote sensing of ice clouds. Part II: Narrowband models,” *J. Appl. Meteorol.* **44** (12), 1896–1911 (2005).
 42. B. A. Baum, P. Yang, A. J. Heymsfield, A. Bansemmer, A. Merrelli, C. Schmitt, and C. Wang, “Ice cloud bulk single-scattering property models with the full phase matrix at wavelengths from 0.2 to 100 μm ,” *J. Quant. Spectrosc. Radiant. Transfer* **146**, 123–139 (2014).
 43. T. B. Zhuravleva, “Effect of shape and sizes of crystal particles on angular distributions of transmitted solar radiation in two sensing geometries: Results of numerical simulation,” *Atmos. Ocean. Opt.* **34** (1), 50–60 (2021).
 44. K. Sassen, Z. Wang, and D. Liu, “Global distribution of cirrus clouds from CloudSat/Cloud-Aerosol Lidar and Infrared Pathfinder Satellite Observations (CALIPSO) measurements,” *J. Geophys. Res. D* **113** (8), 347–348 (2008).
 45. A. Macke, P. N. Francis, G. M. McFarquhar, and S. Kinne, “The role of ice particle shapes and size distributions in the single scattering properties of cirrus clouds,” *J. Atmos. Sci.* **55** (17), 2874–2883 (1998).
 46. V. N. Skorinov and G. A. Titov, “On the accuracy of an approximation of method for radiant flux calculation under discontinuous clouds,” *Izv. Akad. Nauk SSSR. Ser. Fiz. Atmos. Okeana* **20** (3), 263–270 (1984).

Translated by O. Bazhenov